

Nonenzymatic electrochemical sensing of hydrogen peroxide based on a polyaniline-MnO₂ nanofiber-modified glassy carbon electrode

Jong-Hyeok Lee¹ · Hun-Gi Hong¹

Received: 14 April 2015 / Accepted: 11 August 2015 / Published online: 19 August 2015
© Springer Science+Business Media Dordrecht 2015

Abstract We report the synthesis of polyaniline-manganese dioxide (PANI-MnO₂) nanofibers and their applications as nonenzymatic electrochemical sensors for the determination of hydrogen peroxide (H₂O₂). The PANI-MnO₂ nanofibers were synthesized via a one-step mixing process from the as-prepared PANI nanofiber aqueous dispersion and the aqueous solution of KMnO₄. The morphology and chemical composition of the synthesized PANI-MnO₂ nanofibers were characterized by field-emission scanning electron microscopy (FE-SEM), X-ray photoelectron spectroscopy, and X-ray diffraction. A facile electrochemical hydrogen peroxide sensor based on a PANI-MnO₂-modified glassy carbon electrode (PANI-MnO₂/GCE) was fabricated by a drop-casting method, and its electrochemical behavior was investigated using electrochemical impedance spectroscopy (EIS), cyclic voltammetry (CV), and amperometry. The results clearly exhibited good electrocatalytic activity of the PANI-MnO₂/GCE toward H₂O₂ reduction in pH 7.4 phosphate buffer solution (PBS). The nonenzymatic H₂O₂ sensor displayed a wide linear range (5–50 μM and 0.05–10 mM), low detection limit (0.8 μM at S/N = 3), high sensitivity (403.3 μA mM⁻¹ cm⁻²), and negligible interference from ascorbic acid, uric acid, L-cysteine, and glucose at an applied detection potential of -0.4 V (vs. Ag/AgCl).

Keywords Hydrogen peroxide (H₂O₂) · Manganese dioxide (MnO₂) · Polyaniline (PANI) · Amperometry · Sensor

1 Introduction

Hydrogen peroxide (H₂O₂) is not only the most commonly used oxidizing agent in many fields, but it is also naturally produced by living organisms as a by-product of oxidative metabolism. It is therefore one of the most important analytes in pharmaceutical, clinical, environmental, and food-manufacturing applications [1]. Various techniques for accurately determining H₂O₂ levels have been studied, such as titrimetry [2], chemiluminescence [3], fluorescence [4], and spectrophotometry [5]. Among these techniques, electrochemical methods have attracted extensive attention due to their relative instrumental simplicity, low cost, high sensitivity, portability, efficiency, and real-time detection capability [6]. For instance, electrochemical sensors based on enzymes such as horseradish peroxidase [7], catalase [8], cytochrome c [9], and hemoglobin [10] show high selectivity and sensitivity for H₂O₂ determination. However, enzyme-based sensors are unstable, are relatively expensive to manufacture, require complicated immobilization procedures, and are highly sensitive to environmental conditions [11]. Consequently, many researchers have studied the development of nonenzymatic electrochemical H₂O₂ sensors using various inorganic nanomaterials. In particular, transition metal oxides are a promising candidate because they exhibit efficient electrocatalytic disproportionation of H₂O₂ and possess good characteristics such as high surface area, a large number of active sites, low cost, natural abundance, easy preparation, and high thermodynamic stability for the modification of bare electrode surfaces [12]. For example, copper oxide- [13], iron oxide- [14], cadmium oxide- [15], and zinc oxide-modified [16] electrodes display high sensitivity, low detection limits, and rapid response for H₂O₂ determination.

In recent years, manganese dioxide has been widely used as an electrode material for H₂O₂ determination

✉ Hun-Gi Hong
hghong@snu.ac.kr

¹ Department of Chemistry Education, Seoul National University, Seoul 151-748, Korea

[17–27] owing to its excellent catalytic activity toward the decomposition of hydrogen peroxide [28], and the fact that it is an environment-friendly material [29]. Moreover, MnO_2 can be synthesized simply by one-step reduction of KMnO_4 and holds good stability on GCEs [25]. Several types of MnO_2 nanomaterials have been synthesized and used as electroactive catalysts for H_2O_2 detection. For example, fabrication of a novel sensor using $\beta\text{-MnO}_2$ nanorods was reported [19], and the influences of MnO_2 nanomaterial shapes and structures such as rod, belt, and flower structures over the capacity for nonenzymatic sensing of hydrogen peroxide has also been reported [30]. However, the poor intrinsic electronic conductivity of MnO_2 is a significant problem when seeking a performance improvement of MnO_2 -based electrochemical sensors [31]. Furthermore, because MnO_2 dissolution is facilitated by proton insertion reactions as well as a negative working potential [32], the operating conditions of several MnO_2 -based electrochemical H_2O_2 sensors are restricted to strongly alkaline medium [26] or high positive potential regions [17–24]. In addition, at a positive working potential, oxidizable substances such as ascorbic acid and uric acid can interfere with the precision of H_2O_2 determination. To overcome these shortcomings of MnO_2 , various conducting materials such as noble-metal nanoparticles and carbon nanomaterials have been applied in the fabrication of MnO_2 -based electrochemical H_2O_2 sensors [17, 18, 20, 21, 24–27]. Among these conducting nanomaterials, polyaniline (PANI), which is one of the most commonly studied conducting polymers, is a promising material for chemical sensors owing to its easy and facile synthesis, high electric conductivity, environmental stability, and conductance controllability through simple acid/base doping/dedoping chemistry [33]. Moreover, the emeraldine salt produced from doping an emeraldine base with an acid, i.e., the half-oxidation state of PANI, shows high electric conductivity such that the salt is a good candidate for an electrochemical sensor [34]. However, the electric conductivity of PANI depends on the proton concentration because the acid-doping of PANI results from its protonation. Hence, its main disadvantage for use as an electrochemical sensor is a substantial decrease in its electric conductivity above pH 4.

Along these lines, the synergetic effect of a combination of MnO_2 and PANI will be promising and fascinating for application to electrochemical sensors to determine H_2O_2 . Recently, a study reported H_2O_2 sensing by a glassy carbon electrode (GCE) modified with MnO_2 -carbonized nanostructured PANI in pH 7 phosphate buffer solution (PBS) [35], but it was operated at a very high anodic applied potential (+0.75 V vs. saturated calomel electrode). Moreover, neither its sensitivity, nor linear range, nor the effects of interfering contaminants such as ascorbic acid have been addressed.

To the best of our knowledge, reports on the application of an electrochemical H_2O_2 sensor based on conducting polymer- MnO_2 at a cathodic applied potential have been rare. In this study, we synthesized uniform PANI- MnO_2 nanofibers using as-prepared PANI nanofibers in aqueous dispersion and KMnO_4 aqueous solution by one-step mixing. Then, a fabricated PANI- MnO_2 -nanofiber-modified GCE was used as an electrochemical sensor to determine H_2O_2 . It exhibited good electrocatalytic activity toward the reduction of H_2O_2 at pH 7.4. In addition, it displayed wide linear range, low detection limit, high sensitivity, and negligible interference from ascorbic acid, uric acid, L-cysteine, and glucose.

2 Experimental

2.1 Chemicals and reagents

Hydrogen peroxide (H_2O_2 , 30 wt% in H_2O), potassium permanganate (KMnO_4), aniline ($\text{C}_6\text{H}_5\text{NH}_2$), ammonium persulfate ($(\text{NH}_4)_2\text{S}_2\text{O}_8$, APS), potassium ferricyanide ($\text{K}_3\text{Fe}(\text{CN})_6$), potassium ferrocyanide ($\text{K}_4\text{Fe}(\text{CN})_6$), Nafion (5 % in a mixture of low-aliphatic alcohols and water), ascorbic acid, uric acid, and glucose were purchased from Sigma-Aldrich Co. (USA). L-cysteine was purchased from Yakuri Pure Chemicals Co. (Japan). Hydrochloric acid was obtained from Daejung Chemicals Co. (Korea). Methylene chloride was purchased from J.T. Baker (USA). Phosphate buffer solution (PBS) was prepared at 0.1 M by mixing stock solutions of dipotassium hydrogen phosphate (K_2HPO_4) and monopotassium hydrogen phosphate (KH_2PO_4), both of which were obtained from Junsei Chemical Co. (Japan). All chemicals were of analytic reagent grade and were used without further purification. All solutions were prepared with deionized water (DIW) obtained from an ultrapure water purification system (Human Co., Korea) with a resistivity of not less than 18.2 M Ω cm. All measurements were carried out at room temperature.

2.2 Apparatus and measurements

The electrochemical experiments were conducted using a CHI Model 842B (C.H. Instruments, Inc., USA) device with a conventional three-electrode cell. A glassy carbon working electrode (GCE, 3 mm in diameter), purchased from Bioanalytical System (BAS), was used in the preparation of the modified electrode. The counter and reference electrodes used were a platinum wire and an Ag/AgCl electrode filled with 3 M KCl, respectively. Field emission scanning electron microscopy (FE-SEM) measurements were performed on an S-4800 (Hitachi, Japan). X-ray photoelectron spectroscopy (XPS) was performed on an

AXIS–His (Kratos Inc., Japan), and power X-ray diffraction (XRD) patterns were obtained using a New D8-Advance (Bruker, China) diffractometer. All ultrasonic cleanings were performed using a US-2510 Ultrasonic Cleaner (Branson, USA).

2.3 Synthesis of PANI nanofibers

Polyaniline nanofibers were prepared by an interfacial polymerization method [36], which is performed in an aqueous/organic biphasic system. In brief, 3.2 mmol of aniline was dissolved in 10 mL of methylene chloride. Ammonium persulfate (0.8 mmol) as the oxidant was dissolved in 10 mL of 1 M HCl. After the aniline solution was transferred into a 20-ml glass vial, the aqueous oxidant solution was slowly added with a dropping pipette in order for the acidic aqueous layer to be carefully spread onto an equal volume of the organic solution, forming an aqueous organic interface. Within about an hour, the polymerization reaction was complete, and the aqueous layer containing polyaniline turned dark. The aqueous solution was centrifuged. Subsequently, the precipitate was filtered and washed with DIW several times. Finally, the product was dried in an oven at 40 °C for 12 h.

2.4 Synthesis of PANI-MnO₂ nanofibers

PANI-MnO₂ nanofibers were synthesized according to a reported method [37] with a slight modification. In a typical procedure, 5 mg of as-synthesized PANI nanofibers was dispersed in 2.5 mL of DIW. Then, 2.5 mL of a 0.07 M KMnO₄ aqueous solution was added to the above suspension solution, and kept under stirring for an hour. Next, the precipitate was filtered, then washed with ethanol and DIW by centrifugation at 4000 rpm for 15 min, and finally redispersed into 5 mL of DIW for the electrode modification.

2.5 Electrode modification

A GCE was polished using aqueous slurries of successively finer alumina powders (particle size: 0.3 and 0.05 μm) on a polishing pad. The GCE was washed and then sonicated in deionized water for 2 min. After the electrode was dried under a gentle stream of N₂ gas, 6 μL of PANI or PANI-MnO₂ dispersion solution was dropped onto the polished GCE surface. The modified electrodes were dried in an oven at 40 °C for an hour. For comparison, MnO₂/GCE was fabricated using an electrodeposition method [24]. In brief, MnO₂ was electrodeposited onto the surface of a bare GCE by cyclic potential scanning from 0.4 to 1.3 V for 20 cycles in 0.1 M Na₂SO₄ including 5 mM MnSO₄. After

that, 6 μL of Nafion (0.5 wt % in ethanol) was also placed onto all the modified electrode surfaces. Finally, the electrodes were dried in an oven at 40 °C for an hour.

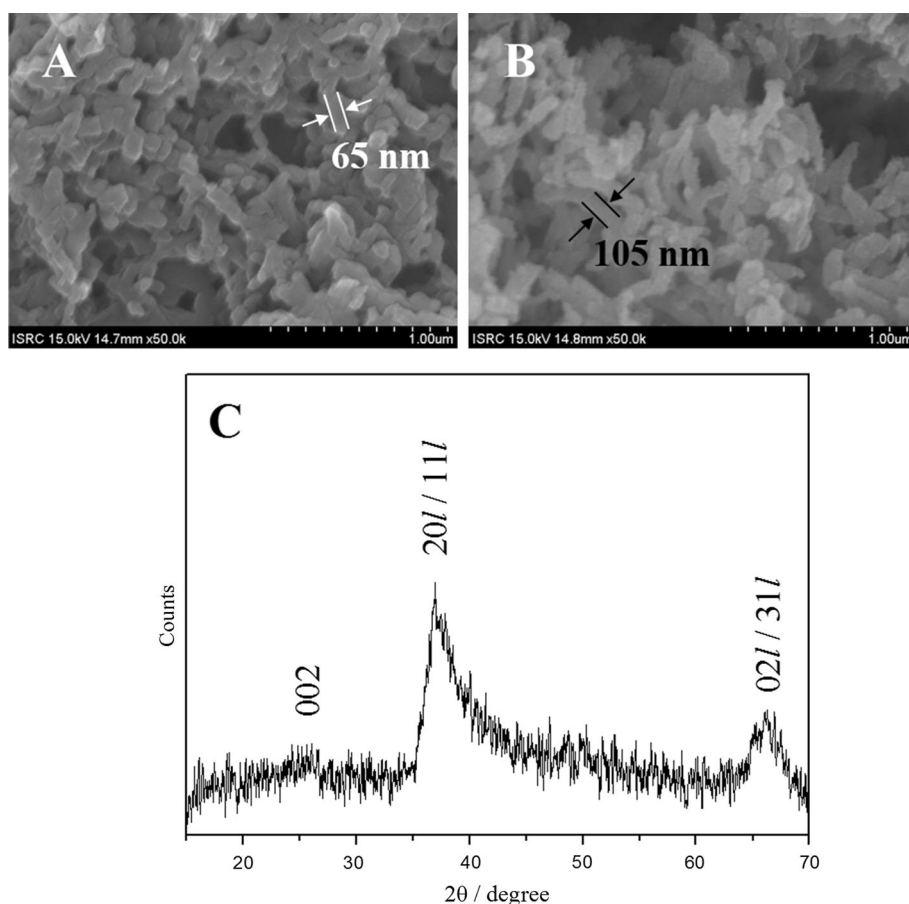
3 Results and discussion

3.1 Characterization of synthesized PANI and PANI-MnO₂ nanofibers

The morphologies of PANI and PANI-MnO₂ nanofibers were characterized by means of field-emission scanning electron microscopy (FE-SEM), as shown in Fig. 1. Figure 1a shows that the PANI nanofibers consist of one-dimensionally uniform interwoven shapes. The average diameter of the PANI nanofibers was estimated to be about ~65 nm. After the MnO₂-coating process, the structure of the nanofibers was preserved well, and the average diameter of the PANI-MnO₂ nanofibers was slightly increased to ca. 105 nm, as shown in Fig. 1b. This clearly indicates that the PANI nanofibers were uniformly coated by a thin layer of MnO₂ and acted as a substrate for the growth of the MnO₂ layer. Figure 1c shows the X-ray diffraction pattern of the PANI-MnO₂ nanofibers obtained under our synthesis conditions. The three observed broad peaks at 2θ of approximately 25°, 37°, and 66° can be assigned to the periodicities of the (002), (20//11), and (02//31) planes in monoclinic potassium birnessite-type MnO₂ (JCPDS no. 80-1098), which has been previously reported [37, 38]. These XRD patterns confirm that the MnO₂ immobilized on the PANI nanofibers seems to be in substantially amorphous phase. According to these reports, the birnessite-type of MnO₂ (δ-MnO₂·nH₂O) consists of a 2D-layered structure with edge-sharing MnO₆ octahedral layers and contains K⁺ cations and water molecules in the interlayer space.

The chemical composition of the as-synthesized nanofibers and the oxidation state of the manganese were investigated by XPS. The XPS survey spectra of the PANI and PANI-MnO₂ are presented in Fig. 2a. Only C, N, and O were present in the PANI sample, whereas the PANI-MnO₂ nanofibers contained C, N, O, and Mn. To further understand the electronic state of the manganese element in the nanofibers, high-resolution XPS spectra were examined. As shown in Fig. 2b, the Mn 2p core-level spectrum shows two peaks at 641.5 and 653.3 eV, corresponding to Mn 2p_{3/2} and Mn 2p_{1/2} peaks, with a spin-energy separation of 11.8 eV. This result coincides well with the reported data of Mn 2p_{3/2} and Mn 2p_{1/2} in MnO₂ [39]. In addition, there is no Mn 2p_{3/2} peak of KMnO₄ at 647 eV in the high-resolution XPS spectra, demonstrating that the permanganate ions have been completely reduced to manganese dioxide by the polyaniline in the PANI nanofiber dispersion solution.

Fig. 1 SEM images of **a** PANI, and **b** PANI-MnO₂ nanofibers. **c** XRD pattern of PANI-MnO₂ nanofibers



3.2 Electrochemical impedance spectroscopy characterization

Electrochemical impedance spectroscopy (EIS) provides important information about the interfacial properties of surface-modified electrodes [40]. Figure 3 presents typical Nyquist plots of bare GCE, PANI/GCE, MnO₂/GCE, and PANI-MnO₂/GCE in 0.1 M PBS (pH 7.4) containing 5 mM [Fe(CN)₆]³⁻ and 5 mM [Fe(CN)₆]⁴⁻ at +0.22 V (vs. Ag/AgCl). The Nyquist plots are fitted by an equivalent circuit (inset shown in Fig. 3). In general, the semicircle's diameter of the Nyquist plot is known to be equivalent to the electron transfer resistance (R_{ct}) of an electrode. As shown, the bare GCE presented the smallest diameter (curve a), indicating low R_{ct} of 85 Ω. When the bare electrode was coated with PANI nanofibers, the resistance increased to 230 Ω (curve b). The increase in the R_{ct} value might be due to a slight decrease in electric conductivity of PANI in the neutral PBS because PANI loses protons that were doped in the acidic condition. Polyaniline is a unique polymer with a reversible acid/base doping process. It is conductive when it is in the acid or doped emeraldine salt form. However, its conductivity decreases in the emeraldine base or dedoped form of PANI [41]. For the MnO₂/GCE, R_{ct} dramatically increased to approximately

1320 Ω owing to the presence of semiconductive MnO₂ (curve c). However, R_{ct} for the PANI-MnO₂/GCE was slightly reduced to approximately 1180 Ω (curve d) due to the aid of the electrically conductive PANI nanofibers on the GCE surface. Consequently, these results show that the PANI-MnO₂ nanofibers were well immobilized on the bare GCE, and PANI enhanced the electron transfer efficiency at the PANI-MnO₂-modified electrode.

3.3 Electrochemical Performance of the PANI-MnO₂/GCE

The electrochemical properties of the modified electrodes were characterized by cyclic voltammetry in 0.1 M PBS (pH 7.4) at a scan rate of 50 mV s⁻¹. Figure 4a displays typical cyclic voltammograms (CVs) for bare GCE, PANI/GCE, and PANI-MnO₂/GCE in N₂-saturated buffer solution in the absence of H₂O₂. The bare GCE and PANI-MnO₂/GCE showed no significant electrochemical responses (curves a and c). For comparison, several MnO₂/GCEs were fabricated using an electrodeposition method [24]. It was found that MnO₂/GCE shows no reproducible CV response because the MnO₂ layer is easily detached from GCE surface as reported for MnO₂ nanorod-modified GCE [27]. However, MnO₂ was

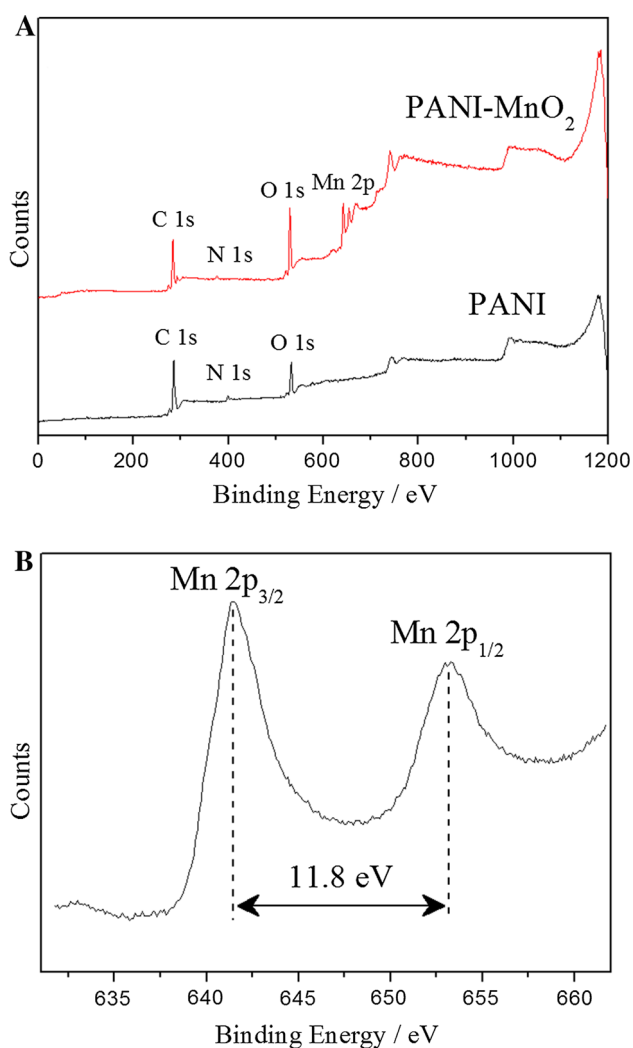


Fig. 2 **a** XPS survey spectra of PANI and PANI-MnO₂. **b** XPS high-resolution spectrum of the Mn 2p core-level in the PANI-MnO₂ nanofibers sample

strongly coated on the large surface area of the PANI nanofibers through chemical reduction of MnO₄⁻ ions. The PANI/GCE showed a pair of broad redox peaks around -0.15 V due to the two state transitions of PANI from leucoemeraldine to emeraldine and from emeraldine to pernigraniline [42] (curve b). Figure 4B displays typical cyclic voltammograms (CVs) for bare GCE, PANI/GCE, and PANI-MnO₂/GCE in N₂-saturated buffer solution in the presence of H₂O₂. The bare GCE and PANI/GCE showed no obvious electrochemical response (curve a and b) related to the electrocatalytic reduction of H₂O₂. However, the PANI-MnO₂/GCE displayed a large reduction peak at -0.45 V (curve c). This result shows that the PANI-MnO₂ nanofiber-modified GCE, unlike the bare GCE and PANI/GCE, has excellent electrocatalytic activity toward reduction of H₂O₂.

Few reports have addressed the possible electrocatalytic mechanism of H₂O₂ reduction at modified electrodes based

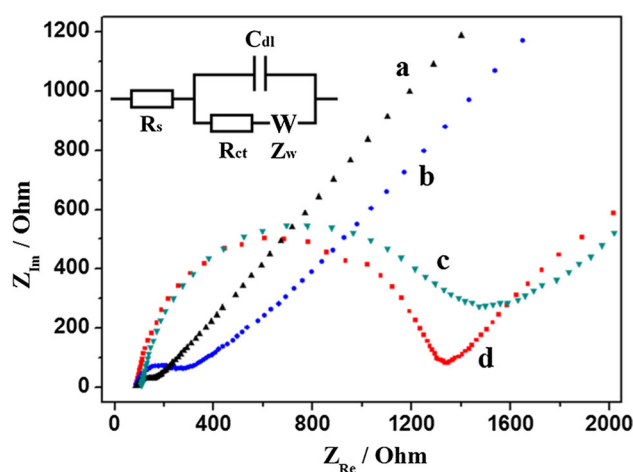


Fig. 3 Nyquist plots of (a) bare GCE, (b) PANI/GCE, (c) MnO₂/GCE, and (d) PANI-MnO₂/GCE in 0.1 M PBS (pH 7.4) containing 5 mM [Fe(CN)₆]³⁻ and 5 mM [Fe(CN)₆]⁴⁻ from 10⁵ to 10⁻² Hz at amplitude of 5 mV. Inset the equivalent circuit

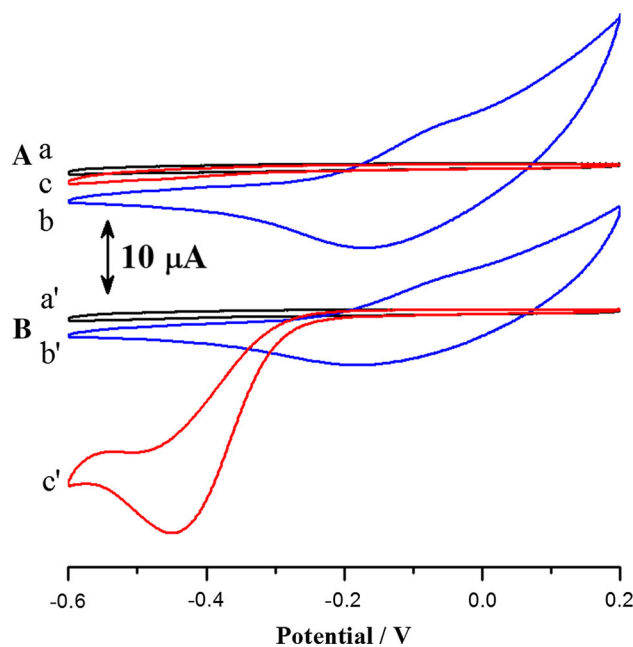


Fig. 4 CVs of (a, a') bare GCE, (b, b') PANI/GCE, and (c, c') PANI-MnO₂/GCE in N₂-saturated 0.1 M PBS (pH 7.4) in the absence (A) and the presence (B) of 1 mM H₂O₂ at a scan rate of 50 mV s⁻¹

on MnO₂ material. For example, Li et al. [26] reported a mechanism based on the redox reaction between MnO₂ and Mn(II) species in strong alkaline conditions using a MnO₂/graphene oxide(GO) nanocomposite-modified GCE. Therein, MnO₂ is reported to be chemically reduced to Mn(OH)₂ species by H₂O₂, and then Mn(OH)₂ is oxidized to MnO₂. Wang et al. [27] proposed another mechanism based on redox reactions between high valence MnO₂ and low valence Mn species such as MnOOH, Mn(OH)₂, or Mn₂O₃ in neutral PBS using a ternary nanocomposite of

Au nanoparticles-MnO₂-reduced GO on GCE. However, the mechanism proposed in the literature [27] is a series of electron transfer reactions among the Mn species in which H₂O₂ does not take part in the redox reaction. The reason that these mechanisms were suggested may be ascribed to the existence of voltammetric redox peaks observed in the absence of H₂O₂. These redox peaks are due to the redox reaction between the low valence Mn pieces Mn(III)–Mn(II). In addition, it was found that both the electrocatalytic oxidation and reduction current at the modified electrodes increased with the concentration of H₂O₂ [26, 27]. However, in this study, no obvious redox peak of Mn species was observed for PANI-MnO₂/GCE in the absence of H₂O₂. This means that the redox reaction between high valence MnO₂ and low valence Mn(II or III) species does not participate in the catalytic mechanism of H₂O₂ reduction by the PANI-MnO₂/GCE. According to earlier studies [43, 44], manganese oxides have been extensively investigated as excellent electrocatalysts for oxygen reduction. To probe the possible electrocatalytic mechanism of H₂O₂ reduction at the PANI-MnO₂/GCE, CVs of O₂ reduction were acquired because the reduction of hydrogen peroxide can be related to the electrocatalytic O₂ reduction. Figure 5a shows a typical cyclic voltammogram for the electrocatalytic reduction of H₂O₂ at the PANI-MnO₂/GCE in N₂-saturated PBS. When the modified electrode was transferred to air-saturated PBS in the absence of H₂O₂, the CV of aerial O₂ reduction was observed at the same negative potential of –0.45 V as shown in Fig. 5b. Here, it is worthwhile to note that the two CVs of Fig. 5a, b are quite similar to each other in terms of wave features such as wave shape and peak potential. From this fact, it is inferable that the possible electrocatalytic H₂O₂ reduction mechanism does not seem to be substantially different from

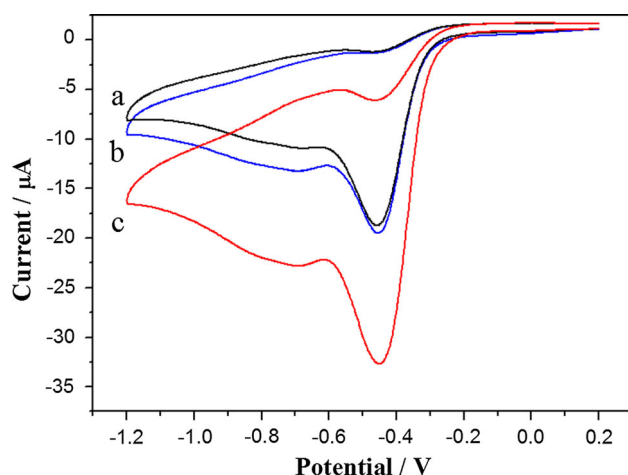
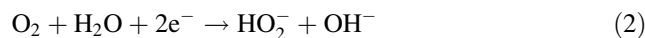
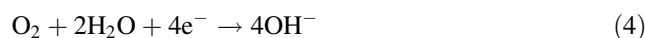


Fig. 5 CVs of PANI-MnO₂/GCE in (a) N₂-saturated, and (b, c) air-saturated 0.1 M PBS (pH 7.4) in the (a, c) presence and (b) the absence of 0.6 mM H₂O₂ at a scan rate of 50 mV s⁻¹

the O₂ reduction mechanism at the surface of the PANI-MnO₂/GCE. Recently, several research groups [43–46] described that O₂ reduction on manganese oxides in neutral and alkaline media occurs through a mechanism involving partial two-electron reduction of O₂ to hydrogen peroxide ion (HO₂⁻) (Eq. 2), which is electrochemically reduced to OH⁻ (Eq. 3) or chemically decomposed to O₂ and OH⁻ (Eq. 3'), and that the overall reaction (I) consists of apparent 4-electron O₂ reduction (Eq. 4).



Overall reaction I:



Overall reaction II:



Herein, we suggest the introduction of a disproportionation reaction of H₂O₂ (Eq. 1) into the O₂ reduction mechanism described above in order to describe the possible electrocatalytic mechanism for the reduction of H₂O₂. However, the disproportionation reaction should be fast enough to not be the rate-determining step of H₂O₂ reduction on the surface of PANI-MnO₂/GCE because manganese oxides are highly catalytically active toward disproportionation. The total reaction of Eqs. 1, 2, and 3 is equivalent to reaction (II) (Eq. 5), which is equivalent to the total reaction of Eq. (1), (2), and (3'). For all, hydrogen peroxide can be said to be electrocatalytically reduced via the electrochemical reduction of molecular oxygen evolved from the disproportionation of H₂O₂ molecules at the surface of MnO₂ nanoparticles deposited on the PANI/GCE.

Figure 5c displays a typical CV observed in air-saturated PBS containing the same concentration of H₂O₂ as in Fig. 5a. The observed large catalytic reduction wave is obviously due to the reduction of dissolved H₂O₂ and aerial O₂. As expected, the CV of Fig. 5c seems to be almost same as the sum of CVs observed in Fig. 5a, b. In addition, it is worth noting that the cathodic peak current value of 34 μA at peak potential of –0.45 V (Fig. 5c) is quite close to the sum of the peak currents at the same potential in Fig. 5a, b, which are 17 and 19 μA, respectively.

We further examined the electrocatalytic activity of the PANI-MnO₂/GCE via changing the H₂O₂ concentration, as shown in Fig. 6A. In the absence of H₂O₂, no obvious peak was present in the background CV. When H₂O₂ was subsequently injected into the N₂-saturated 0.1 M PBS (pH 7.4), the reduction peak current at –0.45 V increased

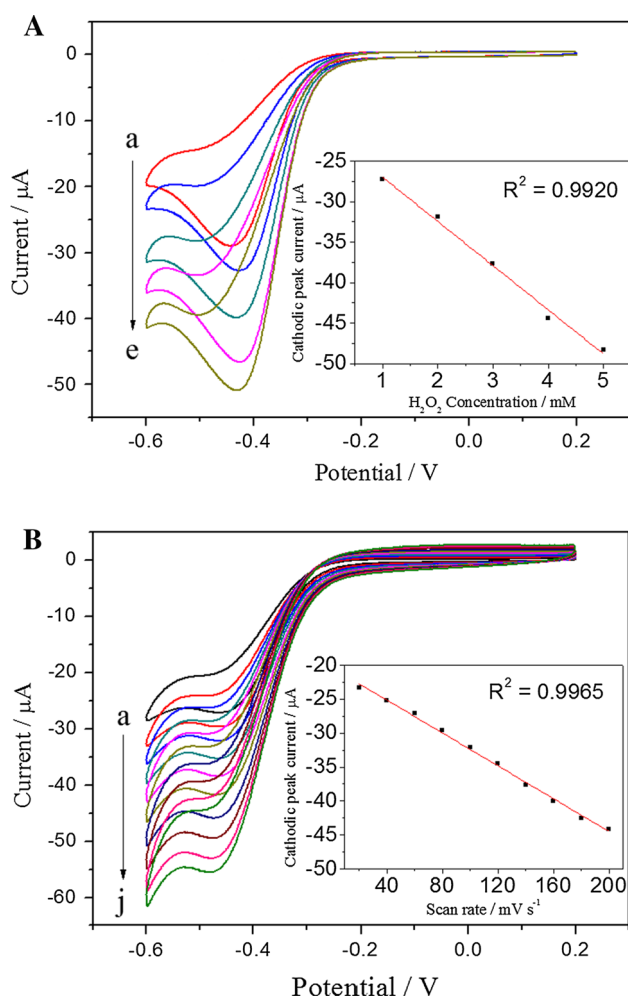


Fig. 6 **A** CVs of PANI-MnO₂/GCE in N₂-saturated 0.1 M PBS (pH 7.4) in the presence of H₂O₂ with different concentrations (from *a* to *e*: 1, 2, 3, 4, and 5 mM) at a scan rate of 50 mV s⁻¹. Inset: plot of the background-corrected cathodic peak current vs. the H₂O₂ concentration. **B** CVs of PANI-MnO₂/GCE in N₂-saturated 0.1 M PBS (pH 7.4) in the presence of 1 mM H₂O₂ at different scan rates (from *a* to *j*: 20, 40, 60, 80, 100, 120, 140, 160, 180, and 200 mV s⁻¹). Inset plot of the background-corrected cathodic peak current of H₂O₂ vs the scan rate

linearly with the increasing H₂O₂ concentration (inset in Fig. 6A), indicating that the PANI-MnO₂ nanofibers are a good electrocatalyst toward H₂O₂ reduction. As seen in Fig. 6B, the cathodic peak current increased with the increasing scan rates ranging from 20 to 200 mV s⁻¹. The electrocatalytic reduction current increased in a linear relationship with the scan rate with a correlation coefficient of 0.9965 (inset in Fig. 6B), indicating that the electrocatalytic reaction process is controlled by the adsorption of H₂O₂. This result is different from a diffusion-controlled process reported in several studies investigating H₂O₂ reduction at low scan rates in neutral PBS using manganese dioxide nanomaterial comprising silver-MWCNT [25], Au-reduced GO [27], or Ag nanoparticles [47]. From our data,

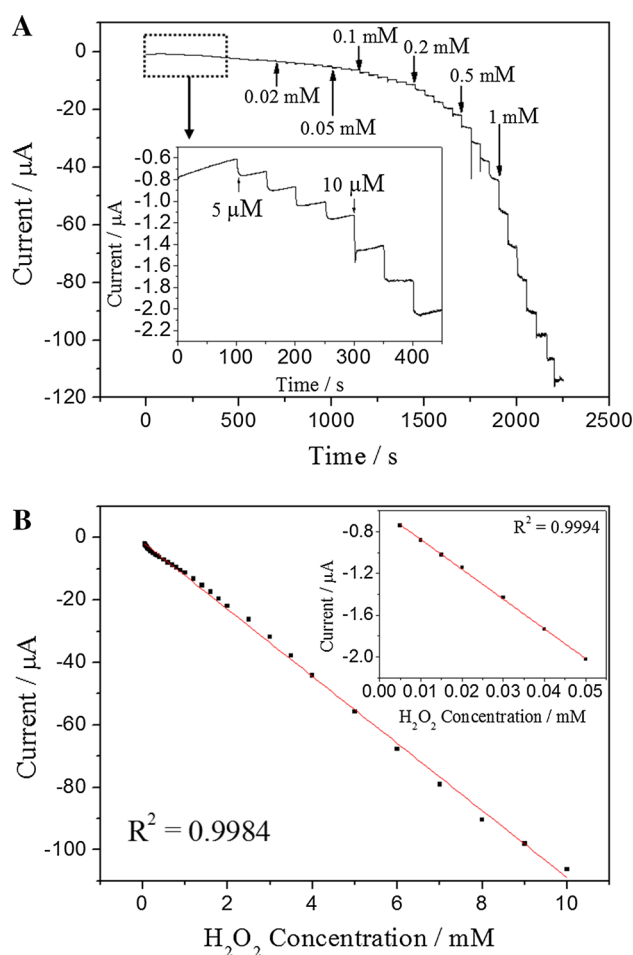


Fig. 7 **a** Amperometric responses of PANI-MnO₂/GCE on successive injections of H₂O₂ into the stirring N₂-saturated 0.1 M PBS (pH 7.4) at -0.4 V. **b** The corresponding calibration curves of the current response versus H₂O₂ concentration. Inset calibration curve in the lower concentration region (from 5 to 50 μM)

we propose that H₂O₂ is initially adsorbed at the surface-active sites of MnO₂ deposited on the PANI nanofibers and then quickly decomposed to H₂O and O₂ (Eq. 1) as described above.

3.4 Amperometric response of PANI-MnO₂/GCE to H₂O₂

Figure 7a displays typical amperometric responses of the PANI-MnO₂/GCE upon successive additions of H₂O₂ into stirred N₂-saturated 0.1 M PBS (pH 7.4) at an applied potential of -0.4 V. A remarkable increase of the reduction current was observed upon subsequent addition of H₂O₂. It is clear that the time required to reach 95 % steady-state current is less than 5 s, indicating rapid amperometric response behavior. This fast response may be ascribed to the excellent electrocatalytic activity of MnO₂ and the electric conductivity of PANI toward the

Table 1 Electroanalytic characteristics of various modified electrodes toward hydrogen peroxide

Electrode	Applied potential (V)	Sensitivity ($\mu\text{A mM}^{-1} \text{cm}^{-2}$)	Linear range (M)	Limit of detection (μM)	Reference
$\text{MnO}_2/\text{Na-montmorillonite}/\text{GCE}$	+0.65 ^a	31.4	5×10^{-7} to 7.5×10^{-3}	0.15	[17]
$\text{MnO}_2\text{-AuNP aggregates}/\text{GCE}$	+0.65	0.053	7.8×10^{-7} to 8.4×10^{-4}	0.05	[18]
$\beta\text{-MnO}_2$ nanorods/GCE	+0.80 ^a	21.74	2.5×10^{-6} to 4.3×10^{-2}	2.45	[19]
$\text{MnO}_2\text{NP-CNFs}/\text{GCE}$	+0.60 ^a	71	1.0×10^{-5} to 1.5×10^{-2}	1.1	[20]
$\text{MnO}_2\text{-DHP}/\text{GCE}$	+0.65 ^a	266	1.2×10^{-7} to 2.2×10^{-3}	0.08	[21]
MnO_2/CFME	+0.58	10.6	1.2×10^{-5} to 2.6×10^{-4}	5.4	[22]
$\text{MnO}_2/\text{VACNTs}$	+0.45	1080	1.2×10^{-6} to 1.8×10^{-3}	0.8	[23]
$\text{MnO}_2/\text{OMC}/\text{GCE}$	+0.45 ^a	806.8	5.0×10^{-7} to 6.0×10^{-4}	0.07	[24]
$\text{Ag-MnO}_2\text{-MWCNT}/\text{GCE}$	-0.30 ^a	82.5	5.0×10^{-7} to 1.0×10^{-2}	1.7	[25]
$\text{MnO}_2\text{-GO}/\text{GCE}$	-0.30 ^a	38.2	5.0×10^{-6} to 6.0×10^{-4}	0.8	[26]
$\text{Au-MnO}_2\text{-rGO}/\text{GCE}$	-0.20 ^a	980	1.0×10^{-7} to 2.2×10^{-5}	0.05	[27]
PANI- MnO_2/GCE	-0.40	101.6	2.2×10^{-5} to 1.26×10^{-2}	0.8	This work
		403.3	5.0×10^{-6} to 5.0×10^{-5}		
		152.1	5.0×10^{-5} to 1.0×10^{-2}		

^a vs. saturated calomel electrode (SCE)

reduction of H_2O_2 , although MnO_2 is intrinsically a poor electronic conductor. The corresponding calibration curves of the reduction peak current vs. the concentration of H_2O_2 are shown in Fig. 7b. It was found that the entire region showing a linear response could be divided into two regions with different slopes. In the lower concentration region from 5 to 50 μM , the estimated sensitivity of the sensor is $403.3 \mu\text{A mM}^{-1} \text{cm}^{-2}$ with a correlation coefficient of 0.9994 (inset in Fig. 7b). However, as shown in Fig. 7b, the sensitivity decreases to $152.1 \mu\text{A mM}^{-1} \text{cm}^{-2}$ in the higher concentration region (from 50 μM to 10 mM) with a correlation coefficient of 0.9984. The limit of detection was estimated to be 0.8 μM at a signal-to-noise ratio of 3. As seen in Table 1, comparing with several typical nonenzymatic sensors based on MnO_2 nanostructures reported previously, the present PANI- MnO_2/GCE showed better performance with regard to the reduction of H_2O_2 in view of its high sensitivity, wide linear range, and low limit of detection. These results can be explained by the high surface area, good catalytic activity, chemical stability, and improved electric conductivity of PANI- MnO_2 nanofibers on a GCE.

3.5 Selectivity, reproducibility, and stability

There are various types of interfering compounds that potentially coexist with H_2O_2 in biological fluids. They were investigated under the experimental conditions optimized for the amperometric determination of H_2O_2 . The interference experiments were performed in N_2 -saturated 0.1 M PBS (pH 7.4) at an applied potential of -0.4 V by comparing the current response to 0.1 mM H_2O_2 with that to each

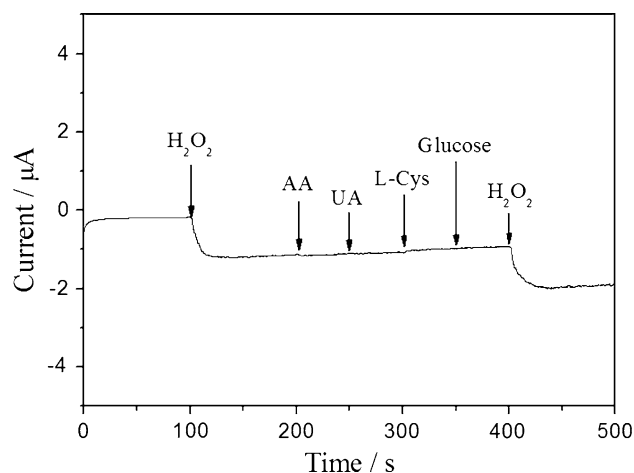


Fig. 8 Amperometric responses of PANI- MnO_2/GCE on successive injections of H_2O_2 , AA, UA, L-Cys, and glucose (0.1 mM, respectively) in N_2 -saturated 0.1 M PBS (pH 7.4) at -0.4 V

interfering substance such as ascorbic acid (AA), uric acid (UA), L-cysteine (L-Cys), and glucose. As shown in Fig. 8, there were no actual amperometric responses of the PANI- MnO_2/GCE upon successive injections of AA, UA, L-Cys, and glucose (0.1 mM, respectively) into N_2 -saturated 0.1 M PBS (pH 7.4), except that the reduction current increased due to H_2O_2 addition. So far, most MnO_2 -based electrochemical H_2O_2 sensors experience significant interference from ascorbic acid owing to their high positive detection potential [17–20]. However, this interference phenomenon is greatly suppressed at the PANI- MnO_2/GCE when the applied potential is switched to -0.4 V. In addition, the interference from other substances is observed to be negligible,

Table 2 Electrochemical determination of H₂O₂ in commercial toothpaste

Experiment no.	Spiked (μM)	Found (μM)	Recovery (%)	R.S.D. (%) ^a
1	54.8	52.8	96.2	5.5
2	273.1	263.3	96.4	5.0

^a R.S.D. (%) calculated from five separate experiments

suggestive of high selectivity. From the measurement of the current responses of five samples of PANI-MnO₂/GCEs in N₂-saturated 0.1 M PBS (pH 7.4) containing 1 mM H₂O₂, we found that the relative standard deviation of the responses was ca. 3.1 %, representing good reproducibility. Furthermore, the average current response of the electrodes remained at 97.6 % of its initial value after 7 days of exposure to air under ambient conditions, indicating good stability. The merits of the prepared sensor demonstrate that the PANI-MnO₂/GCE can be used as an electrochemical sensor for the selective determination of H₂O₂.

3.6 Real sample analysis

In an attempt to evaluate the practical applicability of PANI-MnO₂/GCEs, the electrode was successfully applied to determine H₂O₂ content in a commercial toothpaste. For real H₂O₂ sample preparation, 2.4902 g of toothpaste was dissolved in 10.0 mL of 0.1 M PBS (pH 7.4), yielding a 54.9 mM H₂O₂ sample solution. H₂O₂ samples (10.0 and 50.0 μL) were added to 10.0 mL of 0.1 M PBS, and the current responses were recorded at −0.40 V by amperometry. The recovery rates of H₂O₂ for the two samples were determined by the standard addition method, and the corresponding results are given in Table 2. The average recovery rate based on this method was found to be approximately 96 %, and the R.S.D. of each sample was less than 6 %. These results obtained by amperometry indicate that the proposed electrode is a promising candidate for practical application in the determination of H₂O₂.

4 Conclusion

In summary, PANI-MnO₂ nanofibers were simply synthesized by mixing the as-prepared PANI nanofiber dispersion and the aqueous KMnO₄ solution, and a sensitive nonenzymatic H₂O₂ sensor based on the nanofibers was fabricated. The sensor displays several advantages such as a wide linear concentration range, a low detection limit, good reproducibility, high sensitivity, and long-term stability toward the reduction of H₂O₂. These merits may be attributed not only to the synergistic interaction of the excellent electrocatalytic activity of MnO₂ and the good electric conductivity of PANI, but also to the high surface area of the nanofibers providing more active sites for H₂O₂

adsorption. Moreover, the relatively low detection potential of −0.4 V allows the sensor to exhibit excellent selectivity against several electroactively interfering substances. The proposed PANI-MnO₂/GCE can be used as an amperometric sensor for routine analysis of H₂O₂ in toothpaste samples, which indicates that this nonenzymatic H₂O₂ sensor is a promising candidate for practical applications.

References

- Chen W, Cai S, Ren Q-Q, Wen W, Zhao Y-D (2012) Recent advances in electrochemical sensing for hydrogen peroxide: a review. *Analyst* 137:49–58
- Klassen NV, Marchington D, McGowan HCE (1994) H₂O₂ determination by the I₃[−] method and by KMnO₄ titration. *Anal Chem* 66:2921–2925
- Hanaoka S, Lin J-M, Yamada M (2001) Chemiluminescent flow sensor for H₂O₂ based on the decomposition of H₂O₂ catalyzed by cobalt(II)-ethanolamine complex immobilized on resin. *Anal Chim Acta* 426:57–64
- Li Y, Townshend A (1998) Evaluation of the adsorptive immobilisation of horseradish peroxidase on PTFE tubing in flow systems for hydrogen peroxide determination using fluorescence. *Anal Chim Acta* 359:149–156
- Matsubara C, Kawamoto N, Takamura K (1992) Oxo[5, 10, 15, 20-tetra(4-pyridyl)porphyrinato]titanium(IV): an ultra-high sensitivity spectrophotometric reagent for hydrogen peroxide. *Analyst* 117:1781
- Chen A, Chatterjee S (2013) Nanomaterials based electrochemical sensors for biomedical applications. *Chem Soc Rev* 42:5425–5438
- Wang Y, Ma X, Wen Y, Xing Y, Zhang Z, Yang H (2010) Direct electrochemistry and bioelectrocatalysis of horseradish peroxidase based on gold nano-seeds dotted TiO₂ nanocomposite. *Biosens Bioelectron* 25:2442–2446
- Huang K-J, Niu D-J, Liu X, Wu Z-W, Fan Y, Chang Y-F, Wu Y-Y (2011) Direct electrochemistry of catalase at amine-functionalized graphene/gold nanoparticles composite film for hydrogen peroxide sensor. *Electrochim Acta* 56:2947–2953
- Xiang C, Zou Y, Sun L-X, Xu F (2008) Direct electron transfer of cytochrome c and its biosensor based on gold nanoparticles/room temperature ionic liquid/carbon nanotubes composite film. *Electrochem Commun* 10:38–41
- Guo H-L, Liu D-Y, Yu X-D, Xia X-H (2009) Direct electrochemistry and electrocatalysis of hemoglobin on nanostructured gold colloid-silk fibroin modified glassy carbon electrode. *Sensors Actuators B* 139:598–603
- Mu Y, Jia D, He Y, Miao Y, Wu H-L (2011) Nano nickel oxide modified non-enzymatic glucose sensors with enhanced sensitivity through an electrochemical process strategy at high potential. *Biosens Bioelectron* 26:2948–2952
- Salimi A, Hallaj R, Soltanian S, Mamkhezri H (2007) Nanomolar detection of hydrogen peroxide on glassy carbon electrode

- modified with electrodeposited cobalt oxide nanoparticles. *Anal Chim Acta* 594:24–31
13. Wang B, Luo L, Ding Y, Zhao D, Zhang Q (2012) Synthesis of hollow copper oxide by electrospinning and its application as a nonenzymatic hydrogen peroxide sensor. *Colloids Surf B Biointerfaces* 97:51–56
 14. Liu Z, Zhao B, Shi Y, Guo C, Yang H, Li Z (2010) Novel nonenzymatic hydrogen peroxide sensor based on iron oxide-silver hybrid submicrospheres. *Talanta* 81:1650–1654
 15. Butwong N, Zhou L, Ng-eontae W, Burakham R, Moore E, Srijaranai S, Luong JHT, Glennon JD (2014) A sensitive nonenzymatic hydrogen peroxide sensor using cadmium oxide nanoparticles/multiwall carbon nanotube modified glassy carbon electrode. *J Electroanal Chem* 717–718:41–46
 16. Wang Q, Zheng J (2010) Electrodeposition of silver nanoparticles on a zinc oxide film: improvement of amperometric sensing sensitivity and stability for hydrogen peroxide determination. *Microchim Acta* 169:361–365
 17. Xiao X, Song Y, Liu H, Xie M, Hou H, Li Wang, Li Z (2013) Electrospun carbon nanofibers with manganese dioxide nanoparticles for nonenzymatic hydrogen peroxide sensing. *J Mater Sci* 48:4843–4850
 18. Luo L, Li F, Zhu L, Zhang Z, Ding Y, Deng D (2012) Nonenzymatic hydrogen peroxide sensor based on MnO₂-ordered mesoporous carbon composite modified electrode. *Electrochim Acta* 77:179–183
 19. Wang A-J, Zhang P-P, Li Y-F, Feng J-J, Dong W-J, Liu X-Y (2011) Hydrogen peroxide sensor based on glassy carbon electrode modified with β -manganese dioxide nanorods. *Microchim Acta* 175:31–37
 20. Xu B, Ye M-L, Yu Y-X, Zhang W-D (2010) A highly sensitive hydrogen peroxide amperometric sensor based on MnO₂-modified vertically aligned multiwalled carbon nanotubes. *Anal Chim Acta* 674:20–26
 21. Li Y, Zhang J, Zhu H, Yang F, Yang X (2010) Gold nanoparticles mediate the assembly of manganese dioxide nanoparticles for H₂O₂ amperometric sensing. *Electrochim Acta* 55:5123–5128
 22. Yao S, Xu J, Wang Y, Chen X, Xu Y, Hu S (2006) A highly sensitive hydrogen peroxide amperometric sensor based on MnO₂ nanoparticles and dihexadecyl hydrogen phosphate composite film. *Anal Chim Acta* 557:78–84
 23. Yao S, Yuan S, Xu J, Wang Y, Luo J, Hu S (2006) A hydrogen peroxide sensor based on colloidal MnO₂/Na-montmorillonite. *Appl Clay Sci* 33:35–42
 24. Hocevar S, Ogorevc B, Schachl K, Kalcher K (2004) Glucose microbiosensor based on MnO₂ and glucose oxidase modified carbon fiber microelectrode. *Electroanalysis* 16:1711–1716
 25. Han Y, Zheng J, Dong S (2013) A novel nonenzymatic hydrogen peroxide sensor based on Ag–MnO₂–MWCNTs nanocomposites. *Electrochim Acta* 90:35–43
 26. Li L, Du Z, Liu S, Hao Q, Wang Y, Li Q, Wang T (2010) A novel nonenzymatic hydrogen peroxide sensor based on MnO₂/graphene oxide nanocomposite. *Talanta* 82:1637–1641
 27. Wang L, Deng M, Ding G, Chen S, Xu F (2013) Manganese dioxide based ternary nanocomposite for catalytic reduction and nonenzymatic sensing of hydrogen peroxide. *Electrochim Acta* 114:416–423
 28. Do S-H, Batchelor B, Lee H-K, Kong S-H (2009) Hydrogen peroxide decomposition on manganese oxide (pyrolusite): kinetics, intermediates, and mechanism. *Chemosphere* 75:8–12
 29. Yu G, Hu L, Vosgueritchian M, Wang H (2011) Solution-processed graphene/MnO₂ nanostructured textiles for high-performance electrochemical capacitors. *Nano Lett* 11:2905–2911
 30. Babu KJ, Zahoor A, Nahm KS, Ramachandran R, Rajan MAJ, Gnana kumar G (2014) The influences of shape and structure of MnO₂ nanomaterials over the non-enzymatic sensing ability of hydrogen peroxide. *J Nanopart Res* 16:2250
 31. Toupin M, Brousse T, Bélanger D (2002) Influence of microstructure on the charge storage properties of chemically synthesized manganese dioxide. *Chem Mater* 14:3946–3952
 32. Bakardjieva S, Bezdička P, Grygar T, Vorm P (2000) Reductive dissolution of microparticulate manganese oxides. *J Solid State Electrochem* 4:306–313
 33. Li D, Huang J, Kaner RB (2009) Polyaniline nanofibers: a unique polymer nanostructure for versatile applications. *Acc Chem Res* 42:135–145
 34. Huang W, Humphrey BD, MacDiarmid AG (1986) Polyaniline, a novel conducting polymer. Morphology and chemistry of its oxidation and reduction in aqueous electrolytes. *J Chem Soc Faraday Trans* 82:2385–2400
 35. Šljukić B, Stojković I, Cvijetićanin N, Ćirić-Marjanović G (2011) Hydrogen peroxide sensing at MnO₂/carbonized nanostructured polyaniline electrode. *Russ J Phys Chem A* 85:2406–2409
 36. Huang J, Kaner RB (2004) A general chemical route to polyaniline nanofibers. *J Am Chem Soc* 126:851–855
 37. Jiang H, Ma J, Li C (2012) Polyaniline–MnO₂ coaxial nanofiber with hierarchical structure for high-performance supercapacitors. *J Mater Chem* 22:16939–16942
 38. Anu PMU, Srivastava R, Satpati B (2013) Simultaneous detection of guanine, adenine, thymine, and cytosine at polyaniline/MnO₂ modified electrode. *Electrochim Acta* 114:285–295
 39. Dong X, Shen W, Gu J, Xiong L, Zhu Y, Li H, Shi J (2006) MnO₂-embedded-in-mesoporous-carbon-wall structure for use as electrochemical capacitors. *J Phys Chem B* 110:6015–6019
 40. Xiao F, Li Y, Zan X, Liao K, Xu R, Duan H (2012) Growth of metal-metal oxide nanostructures on freestanding graphene paper for flexible biosensors. *Adv Funct Mater* 22:2487–2494
 41. Li D, Huang J, Kaner RB (2009) Polyaniline nanofibers: a unique polymer nanostructure for versatile applications. *Acc Chem Res* 42:135–145
 42. Luo J, Chen Y, Ma Q, Liu R, Liu X (2013) Layer-by-layer self-assembled hybrid multilayer films based on poly(sodium 4-styrenesulfonate) stabilized graphene with polyaniline and their electrochemical sensing properties. *RSC Adv* 3:17866–17873
 43. Cheng F, Su Y, Liang J, Tao Z, Chen J (2010) MnO₂-based nanostructures as catalysts for electrochemical oxygen reduction in alkaline media. *Chem Mater* 22:898–905
 44. Mao L, Zhang D, Sotomura T, Nakatsu K, Koshiba N, Ohsaka T (2003) Mechanistic study of the reduction of oxygen in air electrode with manganese oxides as electrocatalysts. *Electrochim Acta* 48:1015–1021
 45. Gong K, Yu P, Su L, Xiong S, Mao L (2007) Polymer-assisted synthesis of manganese dioxide/carbon nanotube nanocomposite with excellent electrocatalytic activity toward reduction of oxygen. *J Phys Chem C* 111:1882–1887
 46. Roche I, Scott K (2010) Effect of pH and temperature on carbon-supported manganese oxide oxygen reduction electrocatalysts. *J Electroanal Chem* 638:280–286
 47. Liu Z, Han Q, Ni P, Liu Z, Dong X, Wang Y, Li Z (2014) Enhanced hydrogen peroxide sensing by incorporating manganese dioxide nanowire with silver nanoparticles. *Electrochem Commun* 38:110–113